In situ electric-field-induced contrast imaging of electronic transport pathways in nanotube-polymer composites

Stephen Jesse,[a] Michael A. Guillorn, Ilia N. Ivanov, Alexander A. Puretzky, Jane Y. Howe, Phillip F. Britt, and David B. Geohegan
Condensed Matter Sciences Division, Oak Ridge National Laboratory, Oak Ridge, Tennessee 37831

(Received 31 May 2005; accepted 1 June 2006; published online 7 July 2006)

An electric-field-induced contrast mechanism for scanning electron microscopy is reported which permits the visualization of embedded nanomaterials inside various matrices with high contrast and high definition. The high contrast is proposed to result from localized enhancement of secondary electron emission from the nanomaterials due to electric-field-induced changes in their work functions. By utilizing a stage that allows *in situ* current-voltage measurements inside a scanning electron microscope, single-walled carbon nanotubes embedded within polymethyl methacrylate films were visualized directly. In addition to the rapid assessment of nanotube dispersion within polymers, electric-field-induced contrast imaging enables the determination of percolation pathways. From the contrast in the images, the relative voltage at all points in the electron micrograph can be determined, providing a new mechanism to understand electronic percolation through nanoscale networks. © *2006 American Institute of Physics*. [DOI: 10.1063/1.2220058]

Carbon nanotubes are being explored as additives to lend both strength and useful electrical properties to polymers. While other conductive additives have fulfilled this role, the large aspect ratio of nanotubes requires much smaller weight loadings to exceed percolation thresholds. Moreover, the unique electronic and optical properties intrinsic to single-walled carbon nanotubes (SWCNTs) make them materials of choice for emerging applications requiring multifunctional polymer nanocomposites.

However, assessing dispersion of SWCNT bundles inside polymers and analyzing the electrical properties of the percolation networks they form have been major obstacles for both the fundamental understanding and the practical application of nanotube-polymer composites. Macroscale electrical measurements of bulk composites[1,2] and probabilistic estimations,[3,4] though useful in determining percolation thresholds, are too blunt a tool to reveal the junction resistance between nanotube bundles and the electronic conduction pathways through the polymer which are responsible for the macroscopic properties. Bottom-up approaches, such as first principle atomic scale modeling, could in theory render useful information for modeling nanotube bundle junctions in polymer composites as they have for single nanotube junctions.[5–7] However, similar calculations are yet intractable for bundle-bundle junctions given the large number of atoms participating in transport and current computation capacity.

In this letter, the mechanism responsible for enhancing the secondary electron yield from biased nanomaterials is described for the first time. It will be shown that it enables high-contrast, high-definition imaging of percolation networks *in situ* during current-voltage measurements within a scanning electron microscope. The experimental technique is described for SWCNT networks inside polymers. In addition, we demonstrate the use of simple image processing used to indicate which nanotubes participate in current flow within the network. A simple model is presented to explain the remarkably high sensitivity of image brightness to surface potential. It will be shown that the surface potential generates very large electric fields in the vicinity of the high curvature surface of the nanotubes that form the conductive pathways. This field modulates the work function of the embedded nanomaterial, which in turn strongly affects its secondary electron emission yield, and is subsequently seen experimentally as a change in local brightness of the conductive pathway.

Nanotube-polymer composite films were prepared by spin casting purified (<0.01 wt % metal), laser-vaporization-grown SWCNTs (Ref. 8) cosolubilized with polymethyl methacrylate (PMMA) in *ortho*-dichlorobenzene (ODCB). A dispersed suspension of SWCNTs in ODCB was prepared by 20 min of gentle sonication. ODCB provided the best dispersion of the highly purified, strongly bundled SWCNTs used in these studies, and its relatively high boiling point was compatible with spin casting. PMMA/ODCB solutions were prepared separately, stored for several days to allow for the relatively slow solubilization to take place, and finally filtered with a 0.2 μm mesh polyvinylidene fluoride filter to remove any undissolved polymer. The composite solution was prepared by mixing solutions of SWCNT/ODCB (weight loadings between 10 and 100 μg/g) and PMMA/ODCB (1.0–2.0 wt %) together.

Composite solutions were spun cast onto lithographically prepatterned gold electrode structures with minimum separation distances of 1–2 μm. The electrodes were separated from a silicon back gate by a 500-nm-thick SiO_2 layer. Spin casting of the very dilute solutions yielded SWCNT/PMMA composite films that were 40–100 nm thick with weight loadings between 0.1 and 1.0 wt %. The small film thickness was advantageous since the possible conductive pathways were reduced to essentially the two dimensions of the thin film. Hence, the complete topology of the conductive network could be determined from scanning electron microscopy (SEM) micrographs.

High-resolution transmission electron microscope (HRTEM) imaging was performed on composite films formed by spin casting SWCNT/PMMA/ODCB solutions

[a]Electronic mail: sjesse@ornl.gov

 © 2006 American Institute of Physics
Downloaded 27 Jul 2006 to 160.91.90.20. Redistribution subject to AIP license or copyright, see http://apl.aip.org/apl/copyright.jsp

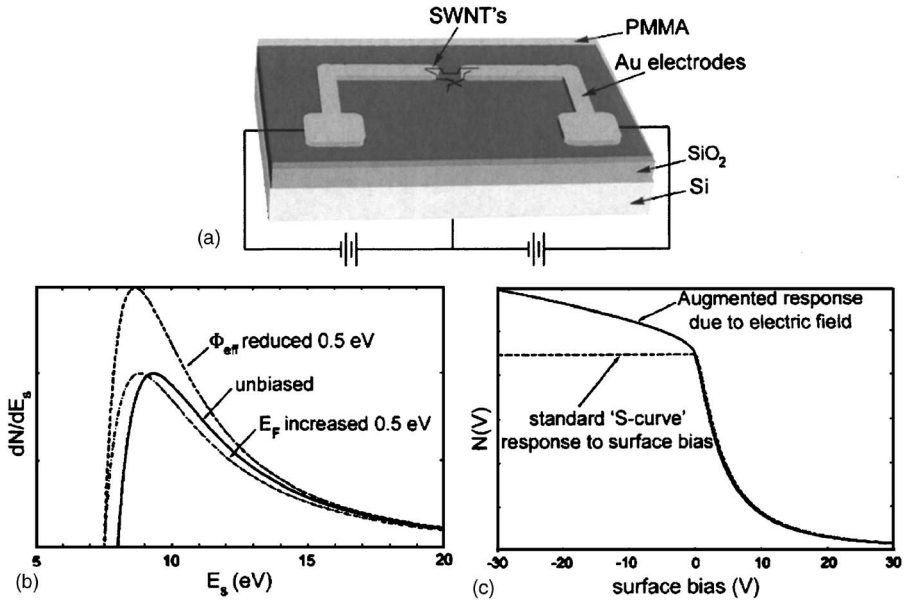

FIG. 1. (a) A schematic of the test structure; (b) plots of Eq. (2) showing effects of shifting Φ_{eff} or E_F on SE spectrum; (c) integrated intensity of SE as a function of surface bias for a typical response where no appreciable electric field is present and the case where surface bias generates an intense electric field and provides an enhanced response. The surface bias axis is offset so that 0 V corresponds to the Fermi energy of the sample.

onto holey carbon grids. While individual SWCNTs or small SWCNT bundles were present, it was determined that nanotubes typically formed into bundles of 10–20 nm diameters.

"Voltage contrast" (VC) is the term generally used to refer to the phenomenon by which a change in surface bias results in a change in brightness[9] as viewed in a SEM. This is a misleading description of what is occurring in the technique outlined here. The sensitivity of brightness to surface bias in this study far exceeds what would be expected by voltage contrast alone in which surface potentials need to be on the order of kilovolts in order to appreciably retard or accelerate high energy incident electrons. In our experiments, small biases (no larger than ±30 V) resulted in significant contrast differences. The small surface voltage does, however, induce a significant electric field (10^7–10^8 V/m) between the conductive path formed by the electrodes and connected nanotubes on the top side of the sample and the silicon back gate beneath. This large electric field is primarily responsible for the image contrast. We therefore propose the term "electric-field-induced contrast" (EFIC). VC results when surface bias has an appreciable influence on the primary electron (PE) beam. EFIC effects are instead due to changes in secondary electron (SE) emission and detection per electric-field-induced modulation of material work function.

Large electric fields (10^7–10^8 V/m) are generated between the conductive path and silicon back gate, causing a shift in the effective work function of the conductive path. This subsequently changes the emission characteristics of biased regions and can be understood by considering the Schottky effect [Eq. (1)],[10] the spectrum of SE [Eq. (2)],[11] and the integrated intensity of SE (sometimes referred to as the "*S* curve") found by integrating Eq. (2) over E_s [Eq. (3)],

$$\Phi_{\text{eff}}(V_s) = \Phi - \sqrt{\frac{q^3}{4\pi\varepsilon}E(V_s)}, \tag{1}$$

$$\frac{d}{dE_s}N(E_s,\Phi_{\text{eff}},E_F) = k\left|\frac{(E_s - E_F - \Phi_{\text{eff}})}{(E_s - E_F)^4}\right|, \tag{2}$$

$$N(V_s) = \frac{k}{6}\frac{\Phi_{\text{eff}}(V_s) + 3V_s}{[\Phi_{\text{eff}}(V_s) + V_s]^3}. \tag{3}$$

Equation (1) shows how the effective work function (Φ_{eff}) can be shifted from the material's actual work function (Φ) in the presence of an electric field (E) where q is electron charge and ε is the dielectric permittivity. The electric field is estimated by treating the nanotube bundle as the inner electrode of concentric capacitor plates as shown by

$$E(V_s) = \frac{V_s}{r_{nt}[\ln(d) - \ln(r_{nt})]}, \tag{4}$$

where d is the oxide thickness, r_{nt} is the bundle radius, and V_s is the surface bias of the sample. This is an adequate approximation since we are concerned only with the electric field intensity at the surface of the nanotube. Equation (2) is the Chung-Everhart approximation of SE emission. dN/dE_s is the number of secondary electrons emitted with the energy E_s. E_F is the Fermi energy of the material and k is a relational constant. N is the total number of secondary electrons emitted.

Figure 1(b) illustrates the roles that a material's Fermi energy and work function play in its SE emission. Considering bias alone (and not the electric field it generates) results only in a change of the Fermi level within a conductor. Applying a negative bias would have the effect of shifting the SE spectrum in energy to the right but would not change the shape of the spectrum or the electron emission efficiency. A large enough positive bias can reduce SE emission if the curve is pushed far enough to the left. This is the reason for the sharp drop off in SE yield in Fig. 1(c). However, if the surface bias also happens to generate a significant electric field, as is the case in this study, an appreciable effective change in the work function can occur and the total number of emitted electrons can be strongly enhanced by a relatively small bias. The consequence of this is made clear in Fig. 1(c) where the integrated intensity is plotted against surface bias. Where normally a varying negative surface bias has no effect on brightness, a negative bias which coincidentally generates a strong electric field can.

Downloaded 27 Jul 2006 to 160.91.90.20. Redistribution subject to AIP license or copyright, see http://apl.aip.org/apl/copyright.jsp

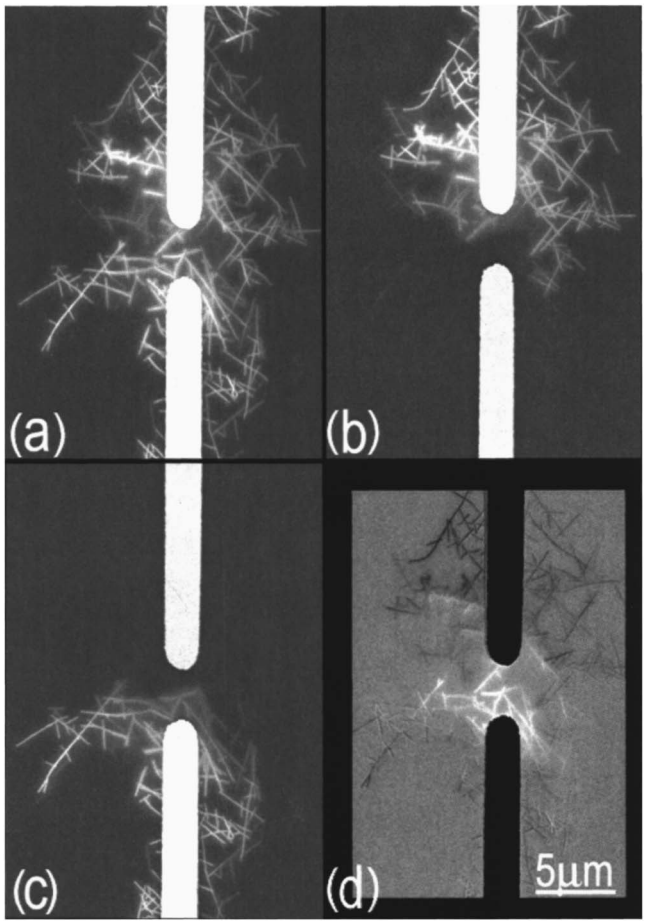

FIG. 2. A series of voltage contrast SEM micrographs under various bias conditions: (a) both electrodes at −20 V, (b) top electrode at −20 V, bottom electrode at ground, and (c) top electrode at ground, bottom electrode at −20 V. (d) Image generated by subtracting (b) and (c) from (a).

The high sensitivity of image brightness to surface potential permits a simple means by which to map surface potential of biased samples. In order to further investigate how charging of the SWCNTs in the polymer might be used to reveal characteristics of the nanotube networks, bias was applied to the network, revealing the nanotube networks and their connective paths.

Figure 2 shows SEM micrographs of the Au electrodes separated by 2 μm in a 0.3 wt % SWCNT/PMMA composite film. When small negative biases (−20 V) are applied to both electrodes [as in Fig. 2(a)], all the nanotubes in contact with both electrodes, or well contacted by these nanotubes, appear brightly in the image. Toward the periphery of the network, marginally connected nanotubes display less contrast.

In order to understand which nanotubes within the network participate in conduction between the two electrodes, one electrode was biased while the other was grounded. As shown in Fig. 2(b), nanotubes connected only to the top electrode (biased at −20 V) appear bright while nanotubes well connected to the grounded electrode are not visible. Nanotubes in shared contact with both electrodes are at an intermediate potential and therefore exhibit an intermediate brightness. Figure 2(c) shows the reverse situation, with the top electrode at ground and the bottom electrode at −20 V. By subtracting Figs. 2(b) and 2(c) from Fig. 2(a), the portions of the nanotube network in shared contact with both electrodes are brought into prominence, as shown in Fig. 2(d). Extraneous nanotubes, which show up strongly in Figs. 2(b) and 2(c), are eliminated from Fig. 2(a). This simple image processing procedure demonstrates that qualitative potential maps of nanotubes embedded in polymer can be measured and that nanotubes participating in current flow can be distinguished from merely attached to one or the other electrode.

This technique can be extended to provide a quantitative potential map throughout the circuit once spectral information about the secondary electron emission is measured. However, the outlined procedure quickly establishes which nanotubes participate in electrical transport as well as their relative degree of participation.

In summary, EFIC is reported as a contrast mechanism in scanning electron microscopy. Local changes in secondary electron yield resulting from field-induced changes in the work function are modeled to explain the high contrast observed for electrically biased SWCNTs inside PMMA observed during current-voltage measurements of nanotube-polymer composite films *in situ* within a SEM. Experimentally, EFIC SEM imaging provides a valuable tool to assess dispersion of carbon nanotubes or other nanomaterials within polymers or other matrices and obtain a great deal of information about their electrical conductivity from the contract in the images. It is possible with this technique to generate voltage potential maps across quasi-two-dimensional (quasi-2D) nanotube percolation networks embedded in thin polymer films, determine the local resistivity in nanotubes, and importantly, determine the junction resistance between nanotubes. EFIC imaging complements scanning probe based techniques[12] and is effective on the length scales where percolation theory breaks down from the loss of statistical significance but that are still too large for atomic scale transport computer simulations to be tractable. Visually mapping the potentials for real networks may be the first step to determine important constants for percolation theory estimates as well as establish bounds for atomic level simulations.

This research was sponsored by NASA-Langley Research Center, the Laboratory-Directed Research and Development Program at ORNL, and the U.S. Department of Energy under Contract No. DE-AC05-00OR22725 with the Oak Ridge National Laboratory, managed by UT-Battelle, LLC.

[1] G. B. Blanchet, C. R. Fincher, and F. Gao, Appl. Phys. Lett. **82**, 1290 (2003).
[2] A. B. Kaiser, G. Dusberg, and S. Roth, Phys. Rev. B **57**, 1418 (1998).
[3] I. Balberg and N. Binenbaum, Phys. Rev. B **28**, 3799 (1983).
[4] I. Balberg, N. Binenbaum, and N. Wagner, Phys. Rev. Lett. **52**, 1465 (1984).
[5] A. Buldum and J. P. Lu, Phys. Rev. B **63**, 161403 (2001).
[6] M. S. Fuhrer, J. Nygard, L. Shih, M. Forero, Y. G. Yoon, M. S. C. Mazzoni, H. J. Choi, J. Ihm, S. G. Louie, A. Zettl, and P. L. McEuen, Science **288**, 494 (2000).
[7] Y. G. Yoon, M. S. C. Mazzoni, H. J. Choi, J. Ihm, and S. G. Louie, Phys. Rev. Lett. **86**, 688 (2001).
[8] D. B. Geohegan, H. Schittenhelm, X. Fan, S. J. Pennycook, A. A. Puretzky, M. A. Guillorn, D. A. Blom, and D. C. Joy, Appl. Phys. Lett. **78**, 3307 (2001).
[9] H. Seiler, J. Appl. Phys. **54**(11), R1 (1983).
[10] S. O. Kasap, *Principles of Electronic Materials and Devices*, 2nd ed. (McGraw-Hill, New York, 2001).
[11] M. S. Chung and T. E. Everhart, J. Appl. Phys. **45**, 707 (1974).
[12] S. V. Kalinin, S. Jesse, J. Shin, A. P. Baddorf, M. A. Guillorn, and D. B. Geohegan, Nanotechnology **15**, 907 (2004).

Downloaded 27 Jul 2006 to 160.91.90.20. Redistribution subject to AIP license or copyright, see http://apl.aip.org/apl/copyright.jsp